

# Hybrid Delta Tracking Schemes Using a Track-Length Estimator

Joanna Piper Morgan<sup>1\*†</sup>    Ilham Variansyah<sup>2</sup>    Kayla B. Clements<sup>2‡</sup>  
 Todd S. Palmer<sup>2</sup>    Kyle E. Niemeyer<sup>1§</sup>

<sup>1</sup>School of Mechanical, Industrial, and Manufacturing Engineering, Oregon State University, Corvallis, OR, 97331, USA

<sup>2</sup>School of Nuclear Science and Engineering, Oregon State University, Corvallis, OR, 97331, USA

## Abstract

In Monte Carlo radiation transport calculations, Woodcock-delta tracking is a common alternative to the more popular surface tracking technique, where the largest cross section at a given energy in a problem is used to sample the distance to collision at any point. Because this process forces extra nonphysical collisions, it is paired with rejection sampling to determine real events from phantom events. Standard implementations of delta tracking preclude the use of a track- (or path-) length estimator for scalar flux tallies, instead using the often higher-variance collision estimator. No mathematical reason prohibits use of the track-length estimator with delta tracking; however, algorithmic inefficiencies have made this combination rare. In this work we introduce a delta-tracking algorithm that tallies fluxes to a structured rectilinear mesh using the track-length estimator. This development also enables hybrid surface-delta tracking algorithms, because the track-length tally can be used everywhere for scalar flux estimation regardless of which tracking algorithm is employed. We use this tallying technique to develop a novel hybrid-in-energy method, where delta tracking is used for high-energy particles (where mean free paths are long) and surface tracking is used for resonance energies and below. We also implement a hybrid-in-material method, similar to what is implemented in Serpent2. We demonstrate that these delta tracking algorithms can be used in conjunction with continuously moving surfaces. We compare these methods showing figures of merit on four time-dependent problems (two multi-group and two continuous energy) solved with CPU- and GPU-based computers. Our implementation of delta tracking with a track length tally modestly improves figures of merit compared to standard delta tracking with a collision estimator and surface tracking with a track length estimator ( $1.5\times$ – $2.5\times$ ) for a problem with significant void regions. For both multi-group and continuous energy pressurized water reactor benchmarks, standard delta tracking with a collision estimator performs best. Hybrid-in-energy methods show significant improvements ( $7\times$ – $11\times$ ) for a continuous energy reactor benchmark problem.

## 1 Introduction

Predicting the neutron distribution in space, energy, and time is essential when modeling inertial confinement fusion experiments, pulsed neutron sources, and nuclear criticality safety experiments, among other systems. The behavior of neutrons can be modeled with a Monte Carlo simulation, where particles are created and transported to produce a particle history [1]. The path of a particle and the specific set of events that occur within its history are governed by pseudorandom numbers, known probabilities (e.g., from material data), and known geometries. Data about how

---

\*Contact: morgan83@llnl.gov

†Currently: Nuclear Criticality Safety Division, Lawrence Livermore National Laboratory, Livermore, CA, 94550, USA

‡Currently: TerraPower LLC, Bellevue, WA 98008, USA

§Contact: kyle.niemeyer@oregonstate.edu

particles move and/or interact within the system are tallied to compute quantities of interest with an associated statistical error from the Monte Carlo process.

Two methods are commonly used to sample the random walk in a Monte Carlo neutron transport algorithm: surface tracking [1] and Woodcock delta tracking [2], which we simply call “delta tracking” for the remainder of this work. These two tracking algorithms have complementary performance bottlenecks [3]. In geometrically complex models with many surfaces, surface tracking can require many expensive calculations to find the distance to a nearest surface which delta tracking avoids. In contrast, when delta tracking in models with certain material compositions, the required rejection sampling can dominate computational cost. Furthermore, standard implementations of delta tracking preclude evaluating quantities of interest with a track-length estimator, instead opting for a collision estimator, while surface tracking has no such restrictions [4]. The track-length estimator often provides lower-variance estimates of quantities of interest (see Section 2) [5]. Due to these differences, relative performance of these methods depend on the problem. For a certain class of problems, a hybrid method may allow greater performance than either approach used individually. There have been other recent developments on delta tracking—namely weighted delta tracking algorithms [6, 3]—but in this work we explore variants of the non-weighted version.

Previous research into hybrid delta-surface tracking on a structured mesh showed good performance for problems with complex arrangements of optically thin materials [7]. However, this work was limited to problems that define material regions and track on a structured mesh. Making material-based decisions about when to use delta and surface tracking has also been explored and implemented in production Monte Carlo codes [8, 9, 10]. Here, we extend the idea of *tracking* on a structured mesh to full delta tracking (eliminating the distance-to-surface check almost entirely) and *tallying* to a structured mesh, allowing the relatively efficient use of a track-length estimator for scalar flux. We describe, verify, and evaluate the performance of a delta-tracking algorithm that allows the use of a track-length estimator on a structured tally mesh.

We then implement this delta tracking plus track length estimator combination in two hybrid delta-tracking schemes: one in which the choice of tracking algorithm is based on the material region, and another based on the particle energy. We implement this work in Monte Carlo / Dynamic Code (MC/DC), an open-source Monte Carlo neutron transport application designed to conduct rapid numerical methods development, specifically for time-dependent problems [11]. We compute figures of merit for four computationally difficult benchmark problems and run-time results for a whole CPU node (two Intel x86 Xeon Sapphire Rapids CPUs) and a whole GPU node (four Nvidia Tesla V100 GPUs) of supercomputing systems at Lawrence Livermore National Laboratory.

This work demonstrates the first published use of a track-length estimator for scalar flux with full delta tracking, the first use of delta tracking in conjunction with continuously moving surfaces, and the first use of a hybrid delta-tracking method based on particle energy. The methods we present here will not be used to compute reaction rate tallies. While this does limit the general applicability of these methods, scalar flux is a necessary quantity for hybrid methods (e.g., iterative quasi Monte Carlo [12, 13]) and other uses.

## 2 Tracking Algorithms and Estimators

Conducting Monte Carlo calculations in problems with heterogeneous materials requires some method of treating discontinuities in the cumulative probability distribution function [14]. This is done with a tracking (or sampling) method. The first method we consider is surface tracking, described in Algorithm 1. For a particle in material  $m$ , the distance to collision is sampled from a cumulative probability distribution function by

$$d_{\text{collision}} = \frac{-\ln(\xi)}{\Sigma_{t,m}(E)}, \quad (1)$$

where  $\Sigma_{t,m}(E)$  [ $\text{cm}^{-1}$ ] is the macroscopic total cross section at a given energy  $E$  of the material  $m$  and  $\xi$  is a pseudorandom number between zero and one.

This sampling of the cumulative probability distribution function will only hold true while the particle is in material  $m$ . If the distance to collision is beyond a material interface in a system with multiple materials, the particle must be stopped at that interface surface and a new distance to collision is sampled using the new material's  $\Sigma_{t,m}(E)$ . This approach is an unbiased way to deal with the sampling of the distance to collision in a heterogeneous medium. In a standard surface-tracking algorithm, both the distance to collision ( $d_{\text{collision}}$ ) and the distance to the nearest surface along the particle's direction of travel ( $d_{\text{surface}}$ ) are computed, and the smaller of these two distances determines which event happens to the particle: a collision or a surface crossing. After or while the particle is moving, tallies can be accumulated to compute quantities of interest. If a collision occurs, more sampling and associated operations are performed (e.g., isotropic scattering of a particle off a particular constituent nuclide). If the particle is still alive and has not exited the problem domain, the algorithm is repeated. The computation of the distance to the nearest surface can become quite expensive as geometries grow in complexity (e.g., complex combinatorial solid geometries (CSG) or CAD-based surfaces). Surface tracking is at the heart of many modern Monte Carlo neutron transport applications, including MCNP [15], Shift [16, 17], MONK/MCBEND [10], COG [18], TRIPOLI-4 [19], and OpenMC [20].

---

**Algorithm 1** A generic surface tracking algorithm.

---

```

1:  $m =$  look up material in current particle location
2:  $\Sigma_{t,m} =$  look up total macroscopic cross section of material  $m$ 
3: while particle is alive do
4:    $d_{\text{collision}} = -\ln \xi / \Sigma_{t,m}$ 
5:    $d_{\text{surface}} =$  compute distance to nearest surface along particle direction of travel
6:   if  $d_{\text{collision}} < d_{\text{surface}}$  then
7:      $d = d_{\text{collision}}$ 
8:     sample collision type
9:     carry out collision
10:  else
11:     $d = d_{\text{surface}}$ 
12:    move particle to surface
13:     $m =$  lookup material on the other side of the surface
14:     $\Sigma_{t,m} =$  look up total macroscopic cross section of material  $m$ 
15:    if surface is a boundary then
16:      implement boundary condition
17:    end if
18:  end if
19:  score  $d$  track lengths to tally bins
20: end while

```

---

Delta tracking is the next most common tracking approach, shown in Algorithm 2. It starts by pre-processing a *majorant* macroscopic cross-section

$$\Sigma_{\text{maj}}(E) = \max(\Sigma_{t,1}(E), \Sigma_{t,2}(E), \dots, \Sigma_{t,m}(E), \dots, \Sigma_{t,M}(E)) , \quad (2)$$

where  $M$  is the total number of materials in the simulation, such that the majorant is the largest cross section in any material in the problem. Cross section data libraries for surface tracking codes often have separate energy grids specialized to each individual nuclide. To compute the correct macroscopic majorant cross section we use a two-step interpolation method. First, we compute the macroscopic total cross section of each nuclide in a given material, then unify the energy grid and interpolate all cross-section points onto that grid. This is repeated when going from single materials to an energy grid for all materials within a problem. The algorithm implemented in MC/DC is shown in Appendix A. Figure 1 shows a macroscopic majorant cross section for a typical pressurized water reactor as a function of neutron energy. When using delta tracking, the distance to collision

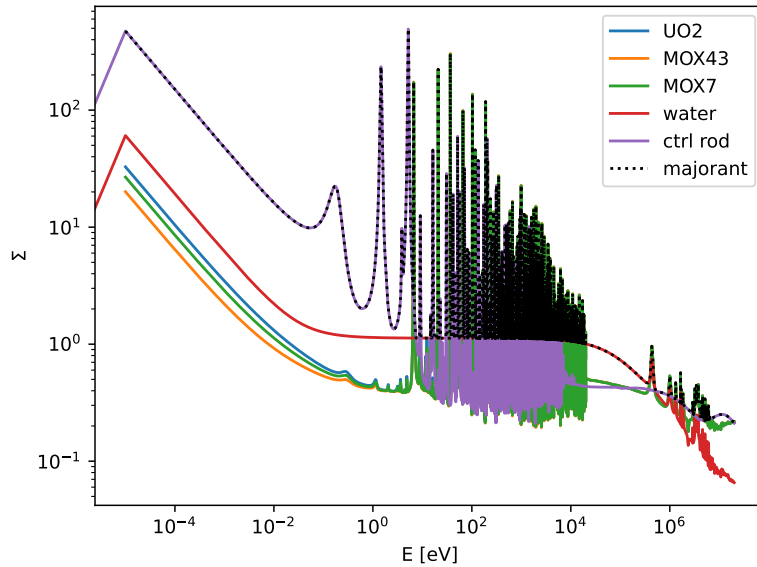


Figure 1: Continuous energy macroscopic majorant cross-section  $\Sigma_{\text{maj}}(E)$  and other material cross-sections for the continuous energy version of C5G7 pressurized water reactor described in Appendix B.

is always sampled with the majorant,

$$d_{\text{collision}} = \frac{-\ln(\xi)}{\Sigma_{\text{maj}}(E)}. \quad (3)$$

However, this sampling forces extra collisions that do not physically occur; using the majorant generates the smallest distance to collision. Delta tracking algorithms use a rejection sample to determine whether the collision event is real or a “virtual” (sometimes called “phantom”) collision. At the current location of the particle, the true material is identified to compute  $\Sigma_{t,m}$  after a potential collision. If

$$\xi > \frac{\Sigma_{t,m}(E)}{\Sigma_{\text{maj}}(E)}, \quad (4)$$

where  $\xi$  is a new random number, the collision did not physically occur and is rejected, so the particle can be left uncollided, alive with its current direction of travel, weight, and energy. From here, the process is the same as before: tallies are accumulated, collision physics is carried out when appropriate, and the algorithm continues as long as the particle is still alive.

Delta tracking requires some way to kill or reflect particles on vacuum or reflecting boundaries, respectively. In a code that already implements surface tracking, the functionality to track distances to specific surfaces will already exist. So, it is natural when utilizing delta tracking to exclusively compute and assess distances to boundary surfaces. If the number of boundary surfaces is small and/or the surfaces can be represented by simple functions, this calculation is computationally trivial.

An added complication when using delta tracking is that only certain tallies can be efficiently scored. Many estimators can be used to compute quantities of interest (e.g., scalar flux, reaction rates) by tallying events that occur within a given region of phase space. Two common scalar flux estimators are the collision estimator and the track-length (also known as the path length), estimator [1]. Often, tallies are scored into bins on a structured mesh that overlays the surfaces and material regions that a Monte Carlo simulation uses to conduct actual transport operations. The track-length



---

**Algorithm 2** Delta tracking in MC/DC. Notably, we are still surface tracking to boundaries.

---

```

1: while particle is alive do
2:    $d_{\text{collision}} = -\ln \xi / \Sigma_{\text{maj}}$ 
3:    $d_{\text{boundary}} = \text{compute distance to boundary}$ 
4:   if  $d_{\text{collision}} < d_{\text{boundary}}$  then
5:     move particle to collision site
6:      $m = \text{look up material in current particle location}$ 
7:      $\Sigma_t = \text{look up total macroscopic cross section of material } m$ 
8:     if  $\xi > \Sigma_t / \Sigma_{\text{maj}}$  then
9:       collision is rejected
10:    else
11:      collision is accepted
12:      tally  $1/\Sigma_t$  to bin at particle's current location
13:      determine collision type
14:      carry out collision
15:    end if
16:  else
17:    move particle to boundary
18:    implement boundary condition
19:  end if
20: end while

```

---

estimator is

$$\hat{\phi}_n = \sum_{i=1}^I p_{i,n}, \quad (5)$$

where  $\hat{\phi}$  is the scalar flux integrated over a given mesh cell  $n$ ,  $p_{i,n}$  is the track length of particle  $i$  passing through mesh cell  $n$ , and  $I$  is the total number of particles. The collision estimator is

$$\hat{\phi}_n = \sum_{i=1}^I \frac{1}{\Sigma_{t,n}(E)}. \quad (6)$$

The collision estimator will often produce a flux estimate with higher variance compared to the track-length estimator when  $\Sigma_{t,m}$  is small (i.e., optically thin, less-dense materials) and is characterized by a zero tally in a true void region [5, 4]. On the other hand, the track-length estimator will tally into every mesh bin the particle moves through during its random walk. In some problem regimes, more information will be scored for a given number of particle histories, which will result in a tally with lower variance.

The estimators in Eqs. (5) and (6) only apply to flux integrals. Response functions for other reaction rates (e.g., fission rate density) will require knowledge of the macroscopic cross section of that reaction in a given location [14]. In this work, when using the track-length estimator with delta tracking we limit ourselves to flux integrals only. We discuss this further in Section 7.

Delta-tracking algorithms are implemented in many production Monte Carlo neutron transport applications, including Serpent2 [9, 4, 8, 21], MONK/MCBEND [10], IMPC [22], and GUARDYAN [23]. Notably, the MONK Monte Carlo neutron transport code is the direct successor to the GEM code where Woodcock et al. first implemented delta tracking [2].

Modern transport applications often involve only one of these two tracking algorithms, and the implementation of their code base is optimized from there. However, either method of sampling the probability distribution functions is valid for the same system in the same simulation, even at the same location in phase space. Some developers have taken advantage of this logic. For example, Serpent2 Monte Carlo code establishes regions of delta tracking and surface tracking based on the ratio between  $\Sigma_{t,m}$  and  $\Sigma_{\text{maj}}$  and a user-supplied constant  $\in [0, 1]$  (where 0 means delta

tracking only and 1 surface tracking only) [8]. MONK/MCBEND supports material regions inside of which delta tracking is implemented (called hole geometries) for complex materials like stochastically heterogeneous materials (e.g., TRISO fuel elements, aggregate and cement mixtures in concrete) while surface tracking is used elsewhere [10, 24].

### 3 Hybrid Delta Tracking Schemes

In this section, we introduce and verify the voxelized tally structure that allows the implementation in MC/DC of a track-length estimator with delta tracking. We also introduce two hybrid surface-delta tracking schemes that we implemented for time-dependent transport with moving surfaces in MC/DC. The first is a region-based delta tracking method we call “hybrid-in-material” that has been previously explored in other production Monte Carlo neutron transport applications [22, 8]. The second method uses delta tracking only for neutrons with energies above resolved neutron cross-section resonances, where total cross sections are often similar to the majorant, and mean free paths are long relative to nominal system dimensions. This approach is called “hybrid-in-energy”.

#### 3.1 Voxelized Tallies

Standard delta-tracking algorithms do not require information about the material or physical mesh cell a given particle occupies at any moment in transport. Conventional wisdom dictates that repeatedly determining locations, cross sections, and tally bin indices while using delta tracking would be costly and eliminate any benefit to performance that the method provides [5]. However, there is nothing *mathematically* preventing the use of a track-length estimator with delta tracking. Furthermore, if all that is desired as a quantity of interest for a given problem is the scalar flux, no cross-section lookups are needed while tallying—only the physical track length and corresponding bin. This forms the underlying idea behind the voxelized tally method. We investigate whether efficient implementation of tallying allows for effective use of a track length estimator when delta tracking and if this results in a performance benefit.

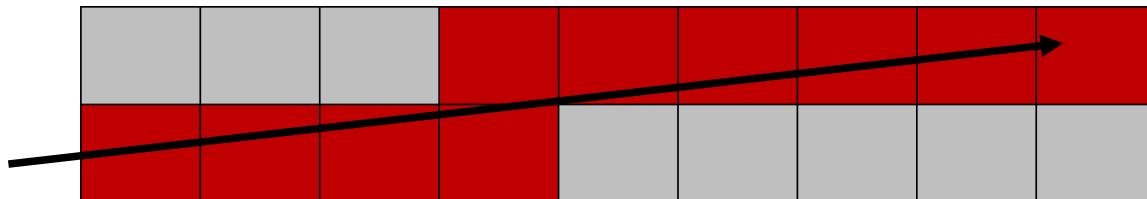


Figure 2: A particle tallying to multiple tally mesh bins (shown in red). Implemented as a single operation for both surface and delta tracking in MC/DC.

As of v0.11.1, MC/DC [11, 25] has a tally algorithm that scores track lengths crossing multiple structured mesh tally bins (voxels) in a single operation. This algorithm is based on a sweep method in which the initial state [mesh cell index,  $(x, y, z)$  position, direction of travel, speed, and particle clock] is known, as is the distance to the next event. The particle is then swept from tally voxel to tally voxel, accumulating the track length traveled in a given voxel along the way. Figure 2 shows a hypothetical particle track and the voxels to be tallied (in red) in a single operation. In MC/DC’s surface-tracking algorithm, this occurs even before moving a particle to an event. This is computationally efficient as we are tallying to a voxel—a structured rectilinear mesh bin.

In this work, we use this voxelized tally scheme when undergoing delta tracking. Even if a particle collision is rejected, that particle still physically moves to the location that was sampled, allowing the use of the track-length estimator. We expect this voxelized tally method to produce scalar fluxes with smaller variance in problems with optically thin regions, where a collision estimator (adapted or otherwise) will not perform efficiently.

To verify that MC/DC’s voxelized track-length tallies with delta tracking converge to the correct solution and at the correct rate, we use four analytic fixed-source benchmark problems from

MC/DC’s verification suite. We compare the error ( $\epsilon$ ) in both the  $L_\infty$  and  $L_2$  norms, from integral quantities of interest to a reference solution and plot the error as a function of increasing particle count. The convergence rate should be the standard Monte Carlo convergence rate of  $N^{-1/2}$ . Our verification problems are:

- AZURV1 time-dependent benchmark both super and sub critical (Figure 3) [26];
- A time-dependent infinite pin cell using the 371 group SHEM cross sections (Figure 4) [27];
- Reed’s problem (Figure 5) [28]; and
- A purely absorbing three-region slab (Figure 6).

All verification simulations show the  $N^{-1/2}$  convergence rate expected for Monte Carlo results. This verifies that we get the expected results with voxelized delta tracking.

### 3.2 Hybrid-in-Material

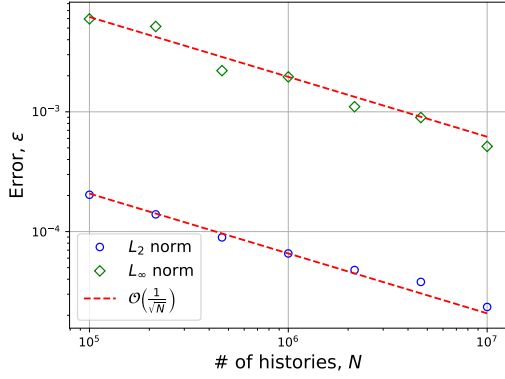
The first hybrid method we implement in MC/DC is the hybrid-in-material method. Each active particle is assigned an additional flag that declares which transport algorithm it is using to sample a distance from the next event. This is similar to Serpent2’s algorithm [4]; however, our voxelized tally structure allows us to use track-length estimators in all regions, not just those in which the particle is undergoing surface tracking. Also, Serpent2’s algorithm makes automatic decisions about where to surface and delta track based on a single user-supplied cut-off value between zero and one for the whole problem [8], whereas we leave it the user to specify on a material-by-material basis. A more automatic approach similar to Serpent2 will be implemented in future work. The IMPC Monte Carlo neutron transport code also implements a similar hybrid-in-material surface-delta tracking scheme [22].

Delta tracking is typically inefficient in systems with strong localized absorbers because particles experience a large number of virtual collisions. For example, Figure 7 shows the cross-section data for the Dragon burst problem we describe in Section 5. This is a simulation that does not warrant delta tracking. This simulation contains three materials, two of which (the fuel and tamper) have similar cross sections over all energies. However, the cross sections for air are over four orders of magnitude lower than the cross sections for the fuel and tamper materials. This means that while particles are delta tracking in the air, they will get stuck in the rejection-sampling loop, statistically rarely completing a particle history. Furthermore, for standard delta tracking (which uses only a collision estimator), the tallies in the air will have higher variance as there will be statistically fewer collisions taking place. Using surface tracking in the air and delta tracking in the material may improve performance in this problem.

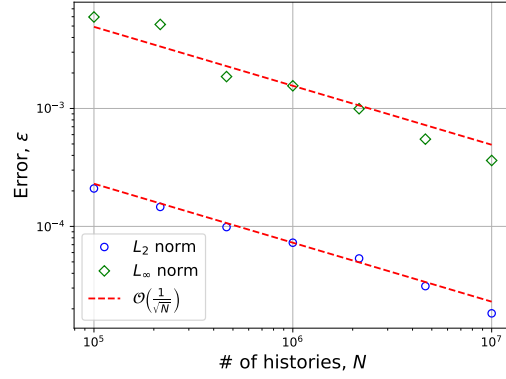
### 3.3 Hybrid-in-Energy

Most high-energy neutron interactions with materials are characterized by relatively long mean free paths (i.e., small cross sections) because they primarily undergo potential scattering [29]. In systems with a large number of surfaces and fast neutrons, delta tracking generally does better compared to surface tracking, because surface tracking gets stuck moving particles from region to region. Delta tracking, on the other hand, will stream particles through the whole problem, never conducting expensive distance-to-nearest-surface computations. Furthermore, at higher energies, cross sections tend to vary less across material interfaces, alleviating issues with the rejection-sampling loop. These observations motivate the development of the “hybrid-in-energy” method that employs delta tracking for high energy neutrons and surface tracking, otherwise.

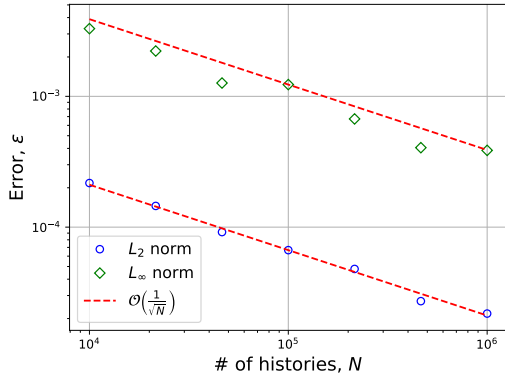
For example, consider a continuous energy version of the C5G7 benchmark reactor geometry [30]. Due to the lack of isotopes available in MC/DC’s cross-section library we replace the guide tube and fission chamber materials with moderator material. We also replace MOX fuels with  $\text{UO}_2$  with different enrichment. The material composition is given by Table 4 in Appendix B. Figure 1 shows



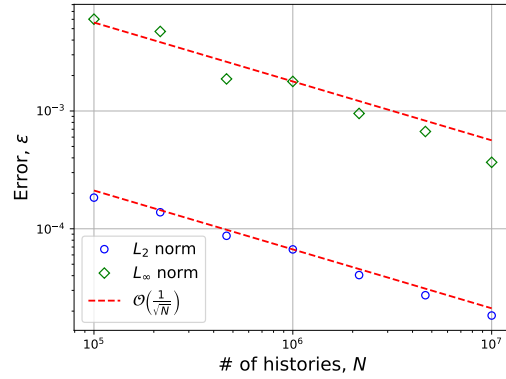
(a) Critical problem with  $\epsilon$  from scalar flux.



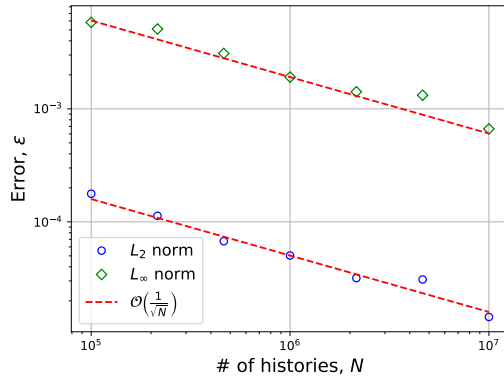
(b) Critical problem with  $\epsilon$  from scalar flux at census.



(c) Subcritical problem with  $\epsilon$  from scalar flux tallies at census.

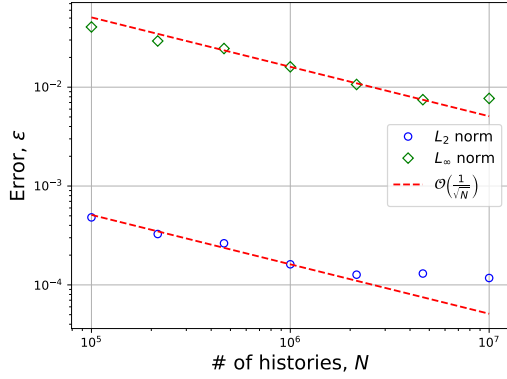


(d) Subcritical problem with  $\epsilon$  from scalar flux.

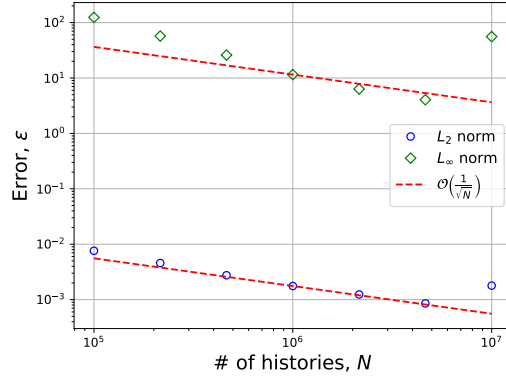


(e) Supercritical problem with  $\epsilon$  from scalar flux.

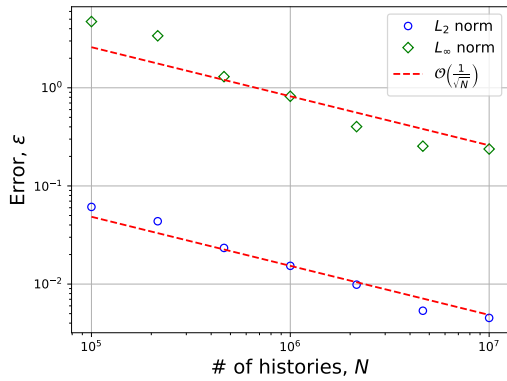
Figure 3: Convergence rate verification of AZURV1 [26], showing the expected Monte Carlo convergence rate ( $N^{-1/2}$ ).



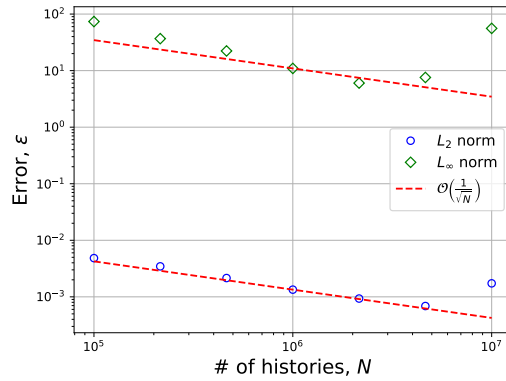
(a) Steady-state problem with  $\epsilon$  from scalar flux.



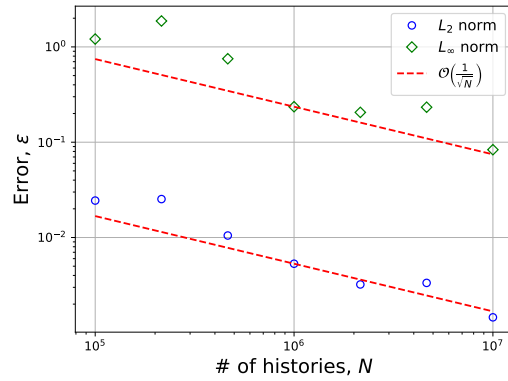
(b) Time-dependent problem with  $\epsilon$  from scalar flux.



(c) Time-dependent problem with  $\epsilon$  from neutron density.



(d) Time-dependent problem with  $\epsilon$  from flux at census.



(e) Time-dependent problem with  $\epsilon$  from neutron density at census.

Figure 4: Convergence rate of an infinite pin using the SHEM 361 group cross section library [27], showing the expected Monte Carlo convergence rate ( $N^{-1/2}$ ).

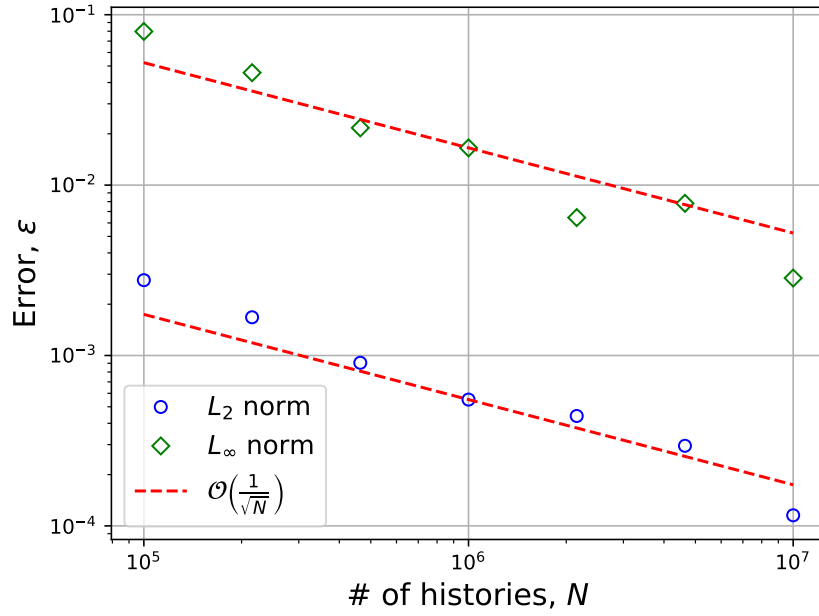


Figure 5: Convergence rate of flux from Reed's problem [28] showing the expected Monte Carlo convergence rate ( $N^{-1/2}$ ).

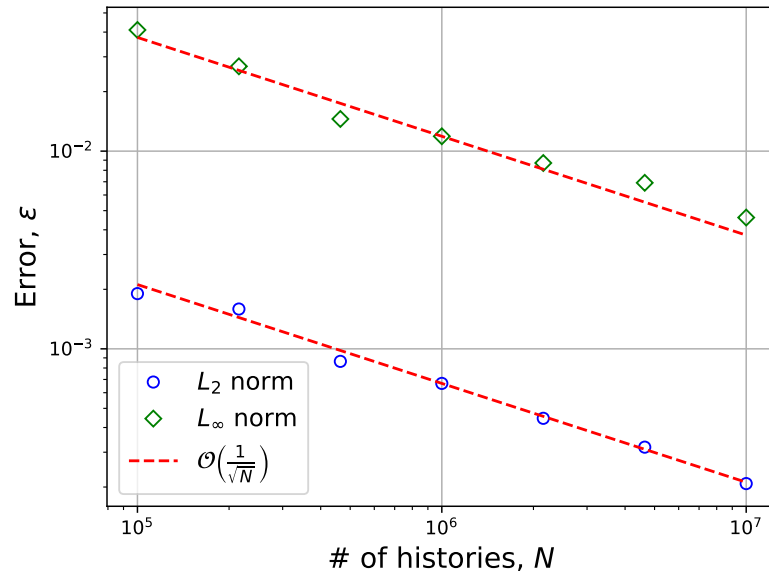


Figure 6: Convergence rate of quantities of interest for a purely absorbing slab wall problem, showing the expected Monte Carlo convergence rate ( $N^{-1/2}$ ).

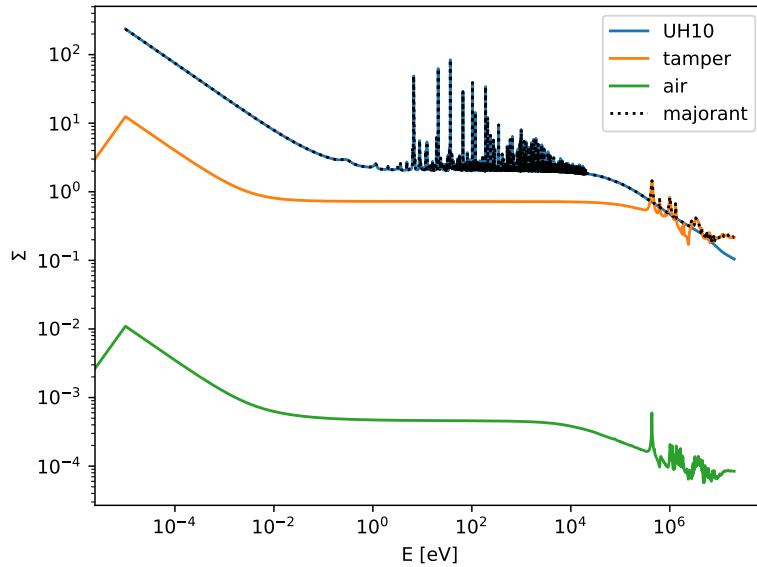


Figure 7: Continuous energy macroscopic majorant ( $\Sigma_{\text{maj}}$ ) and other material cross-sections for the Dragon burst problem.

the macroscopic cross sections for the seven-material reactor, with the majorant in black. Around 10 keV the neutron resonances end and the system is “high energy”.

If using delta tracking for this whole problem, the increased absorption in the resonances of some materials exacerbates issues with the required rejection sampling. Therefore, for this problem, it would be ideal to delta track above 50 keV (to completely avoid neutron resonances) and surface track under that threshold. This forms the basis for our hybrid-in-energy method where both surface and delta tracking are used depending on the energy of individual particles.

### 3.4 Implementation in MC/DC

MC/DC [11] is designed to implement and test new time-dependent Monte Carlo numerical methods at scale [31]. It uses a novel (for the field) development structure in which Python compute kernels are compiled via the Numba just-in-time compiler to run on CPUs and with the Harmonize runtime manager [32, 33, 34] to run on GPUs. MC/DC enables rapid experimentation with these methods at scale on both CPUs and GPUs with time-dependent problems of interest.

Generally, to implement delta tracking in a code that already implements surface tracking, the operations needed are:

1. Pre-process functions to generate a majorant (MC/DC’s implementation is described in Appendix A);
2. Add `if` statements in `distance_to_next_event()` functions to compute relevant distances;
3. Add functions to implement boundary conditions when in delta-tracking mode; and
4. Elevate delta-tracking options to the input deck.

This process is similar to that used to implement hybrid surface-delta tracking methods in MCATK [7]. However, previous work in MCATK implemented a hybrid delta tracking algorithm, which was conceived in part to integrate into MCATK smoothly.

In MC/DC, we have implemented standard delta tracking, delta tracking using voxelized tallies, and two hybrid delta-surface tracking algorithms. Our implementation in total added about 450

lines of code, of which half involved computing various types of majorants (an example can be found in Appendix A). Only about 200 lines of code were required in the compute kernels to implement all considered methods.

When converting a surface tracking code to enable delta tracking, a simple distance-to-nearest boundary function can be produced using existing functionality to find the distance to a nearest surface. In effect, we are still surface tracking—but only to the reflecting boundary surfaces.

## 4 Verification of delta tracking with continuously moving surfaces

To verify that delta tracking can be used in conjunction with continuously moving surfaces in MC/DC, we use the moving pellet test from MC/DC’s regression test suite [11]: a cylindrical fuel element moves through a region that also has a small source. As the pellet moves closer to, then further away from, the source region, the fission rate in the pellet changes. Figure 8 at left shows the fission reaction rate density at various points in time. The outline of the pellet is clearly visible in a number of time steps. These plots were produced using delta tracking with a collision estimator (to compute fission reaction rates).

To further confirm that delta tracking may be used with continuous movement physics, we compare the scalar flux solutions provided from surface tracking and delta tracking with voxelized tallies at various particle counts. We compute

$$\epsilon_N = \left\| \phi_N^{\text{surface}} - \phi_N^{\text{delta}} \right\|_2, \quad (7)$$

where  $\phi_N^{\text{surface}}$  and  $\phi_N^{\text{delta}}$  are scalar flux computed by surface and delta tracking, respectively, at every choice of  $N$  particles. We then compare the norm of the two results over particles to ensure that they converge to the same result at the expected Monte Carlo convergence rate ( $N^{-0.5}$ ). Figure 8 at right shows the norm converging at the expected rate. This regressively verifies that delta tracking can be used in conjunction with continuously moving surfaces. We also produced this same plot for both tracking methods using a collision estimator for both flux and fission reaction rates, all of which match the expected Monte Carlo convergence rate.

## 5 Benchmark Problems

To measure performance, make comparisons, and draw conclusions of the various methods we use benchmark problems—accepted simulations in the radiation transport community. A comparative measurement must be used to take into account both the variance and computation time of a given solution. The figure of merit (FOM) is one such measure. In this work, we will use

$$\text{FOM} = \frac{1}{\hat{\sigma}^2 t_{wc}}, \quad (8)$$

where  $\hat{\sigma}^2$  is the  $L_1$  norm (over phase space) of the variance of the solution provided by the Monte Carlo solver and  $t_{wc}$  is the measured wall-clock runtime the solver took to compute that solution.

We consider four time-dependent fixed-source benchmark problems, comparing the new voxelized tally scheme and hybrid methods proposed to surface tracking methods, on CPU and GPU machines. Two problems are multi-group, and two are continuous energy. Table 1 summarizes the size (in both mesh and particle count) of each benchmark problem. Some problems may not be ideally suitable for delta tracking methods, but are used here to show both correctness under physical problem dynamics (e.g., moving surfaces) and demonstrate algorithmic performance under various physical parameters. All problems are solved with at least four algorithms: surface tracking with a track length and collision estimator, and delta tracking with both a collision and track length estimator. For the C5CE and Dragon burst problem, we also employ a hybrid delta-surface tracking algorithm using the collision and track length tally.



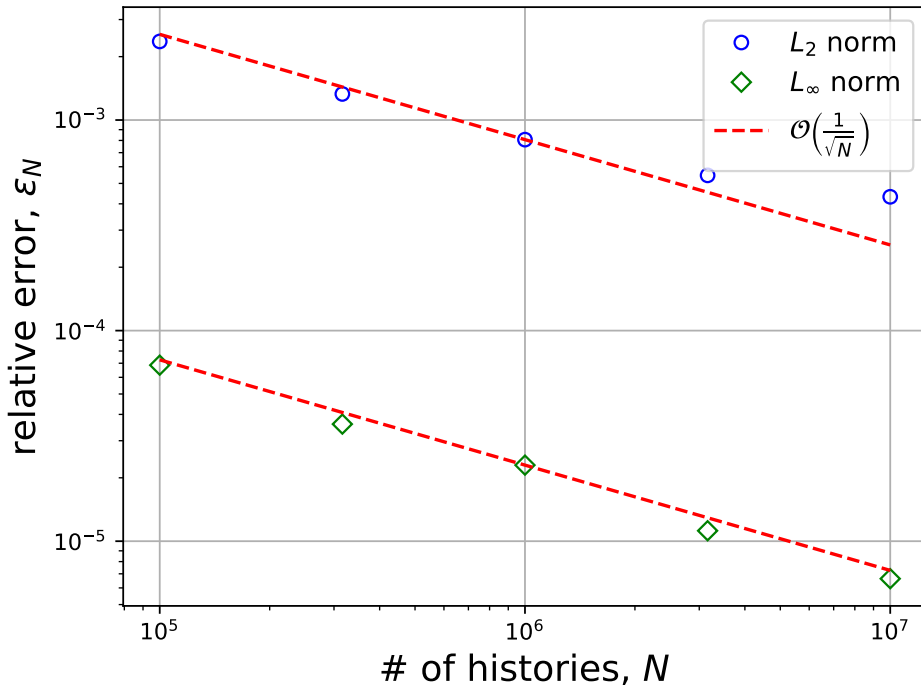
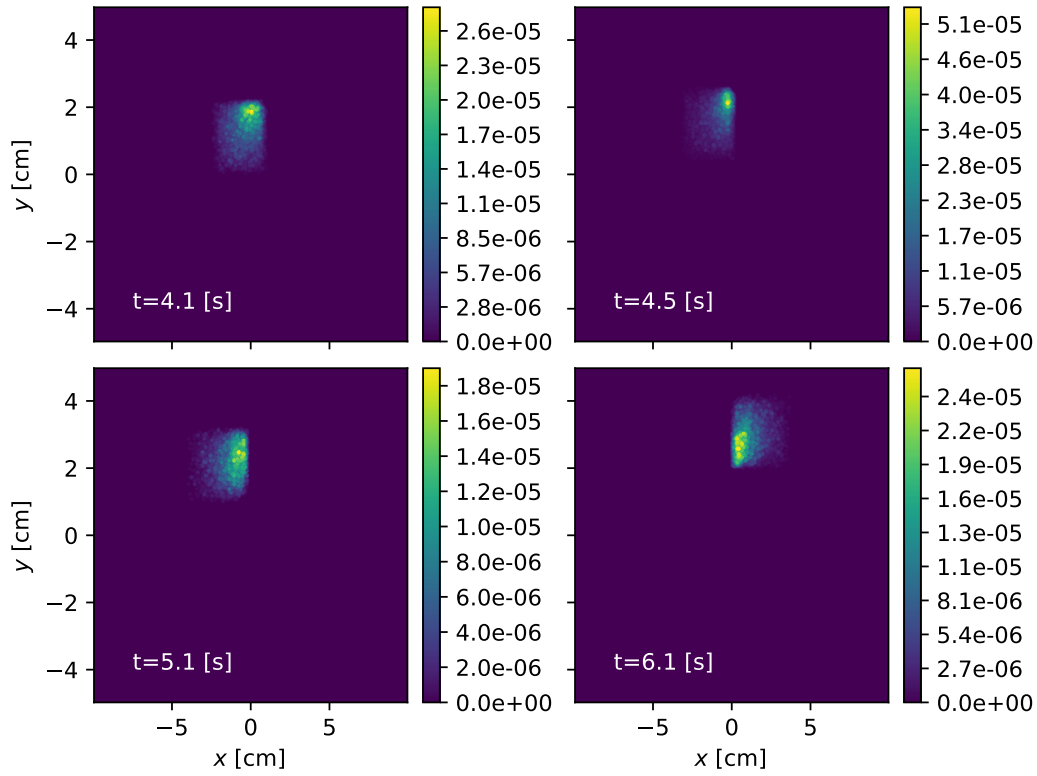


Figure 8: For the moving pellet problem (above) fission reaction rate density at various points in time, (below) convergence between fluxes produced from surface and delta tracking both with the track-length estimator, showing  $N^{-1/2}$  convergence rate.

| Problem      | $N_{\text{mesh}}$ | $N_{\text{particles}}$ | Energy physics                             |
|--------------|-------------------|------------------------|--|
| Kobayashi    | $1.2 \times 10^5$ | $1 \times 10^{10}$     | MG (1 group)                               |
| Dragon Burst | $4.0 \times 10^6$ | $3 \times 10^9$        | CE (3 materials)                           |
| C5G7         | $3.9 \times 10^6$ | $1 \times 10^7$        | MG (7 groups, 8 delayed neutron precursor) |
| C5CE         | $5.4 \times 10^5$ | $1 \times 10^5$        | CE (7 materials)                           |

Table 1: Time-dependent benchmark problems, where “MG” indicates multi-group and “CE” continuous energy.

## 5.1 Kobayashi problem

We first consider a time-dependent version of the Kobayashi problem [35] introduced by Variansyah et al. [31] (a full description is provided by Variansyah [36]). We use 10 batches with  $10^9$  particles per batch ( $10^{10}$  particles total) with surface tracking, standard delta tracking with a collision estimator, and a delta tracking using the voxelized tally method. This problem contains two materials, a low mean-free-path region, characterizing a solid ( $\Sigma = 0.1 \text{ cm}^{-1}$ ), and a high mean-free-path region modeled by air, characterizing a void ( $\Sigma = 1 \times 10^{-4} \text{ cm}^{-1}$ ), in a single energy group. There are  $1.20 \times 10^5$  structured tally voxels in the  $x$ - $y$  plane and in time. For this problem, we expect the voxelized tally method to perform better than standard delta tracking and surface tracking.

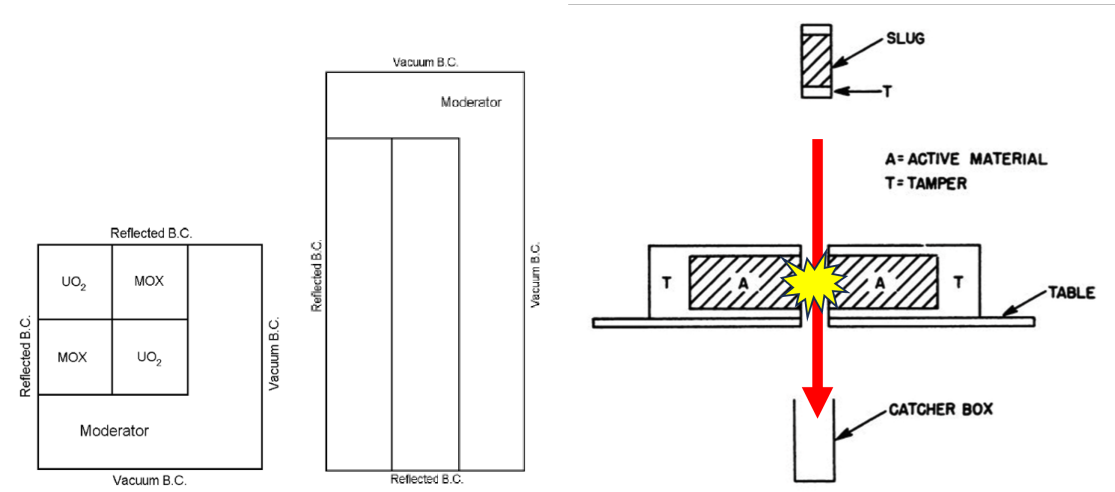


Figure 9: Schematics for benchmark problems: (left) C5G7 reactor quarter (via reflecting boundaries) [30], (right) Dragon burst problem [37].

## 5.2 C5G7 problem

Figure 9 on the left shows the geometry for the next two simulations, which are based on the C5G7 benchmark problem [30]. In energy we use seven energy groups and eight delayed neutron precursor groups. We model a four-phase accident in which a pressurized light water reactor increases in power via the removal of control rods. Figure 10 on the left shows the normalized flux density as a function of time (produced from point reactor kinetics) and the four phases shaded gray, green, red, and blue, respectively. Phase one (shaded gray) starts with the reactor operating in steady state. In phase two (shaded green), the control rods are removed from the reactor to cause the power to increase to a new steady state. Phase three (shaded red) begins when a bank of control rods gets stuck in the fully withdrawn position. Toward the end of phase three, the reactor sees a rapid increase in power that ends at 15s when all control rods are forced into the reactor, ending the accident. In the fourth and final phase, reactor power decays as the delayed neutron population dies out. Figure 10 shows

plots of average flux in the  $x$ - $y$  plane at various points in time, including at 14.95s, the maximum power excursion. These results are from a simulation with  $10^6$  particles in 10 batches (a total of  $10^7$  particles).

We first modeled this problem using the seven-group materials in the C5G7 benchmark description [30], which we call C5G7 in the remainder of this work. We use  $3.9 \times 10^6$  mesh cells in a 3D, time- and energy-dependent tally mesh. The movement of control rods into and out of the reactor is modeled with the continuous movement functionality of MC/DC [38]. To verify the delta tracking methods we explore convergence to the correct solutions using continuously moving surfaces, and we compare delta tracking solutions to solutions provided by surface tracking. This further verifies that delta tracking can be used in conjunction with continuously moving surfaces. Performance data is collected using  $10^6$  particles in 10 batches (total of  $10^7$  particles).

### 5.3 C5CE problem

Next, we define a continuous-energy version of the previous problem (named C5CE), in which the reactor undergoes the same four-phase accident. Table 4 in Appendix B includes the material compositions for the C5CE problem. Using this benchmark, we evaluate both the voxelized tally method and the hybrid-in-energy method described in Section 3.3. Figure 1 shows the macroscopic total and majorant cross sections as a function of energy for the materials in C5CE. The neutron resolved-resonance region ends around 10 keV, so we set the transition energy at 50 keV. Particles moving at energies above 50 keV will use delta tracking, and those below will use surface tracking.

We expect the hybrid-in-energy approach to provide a significant speedup over the other methods explored in this problem, as it avoids the negative impacts of both tracking methods: surface tracking moving from surface to surface and the frequent rejection sampling associated with delta tracking. The C5CE problem includes the same continuously moving surfaces as C5G7, so it serves as an additional verification that delta tracking methods can be used in conjunction with continuously moving surfaces. We model this problem with  $5.44 \times 10^5$  mesh tally bins in a 2D  $x$ - $y$  geometry (integrated along  $z$ ), time and energy-dependent tally mesh. We use  $1 \times 10^5$  particles in a single batch.

### 5.4 Dragon-burst problem

Conducted in 1944 during the Manhattan Project, the Dragon-burst experiments [37] proved that criticality and supercriticality could be achieved with prompt neutrons alone. Previous experiments, such as the Chicago Pile 1, depended on the presence of delayed neutrons to achieve criticality. Figure 9 on the left shows a schematic of the experiment where a highly enriched (75%) uranium hydride slug ( $\text{UH}_{10}$ ) was dropped through a tamper with additional fuel. The slug moves through the core, triggering a prompt supercritical reaction. The reactivity excursion ends when gravity causes the slug to fall out of the core. Kimpland et al. showed that this burst criticality experiment achieved an increase in the neutron population of more than nine orders of magnitude [37]. Here we consider a less-reactive version of the Dragon burst problem (25% enrichment) to test delta tracking with the hybrid-in-material method described in Section 3.2, and to provide additional verification for delta tracking with continuously moving surfaces. Figure 11 shows the overall flux density as a function of time on the left and a  $y$ - $z$  plot of the scalar flux at various points in time on the right.

Figure 7 on the left shows the continuous energy total macroscopic cross sections in the model. The majorant, tamper, and fuel cross sections are almost four orders of magnitude greater than the cross section of air.

We expect delta tracking algorithms to perform quite poorly in this model for a number of reasons. First, when undergoing delta tracking, particles in the air region will experience a large number of rejected virtual collisions, since the majorant is orders of magnitude larger than the cross section of air. Second, as much of the problem involves a near-void material, the collision estimator typically required by delta tracking will generate poor tallies in those regions. Third, the problem is geometrically simple, consisting of a rectangular slug moving through a rectangular slab with a properly sized hole such that the slug can move through the slab. The benefit of delta tracking over

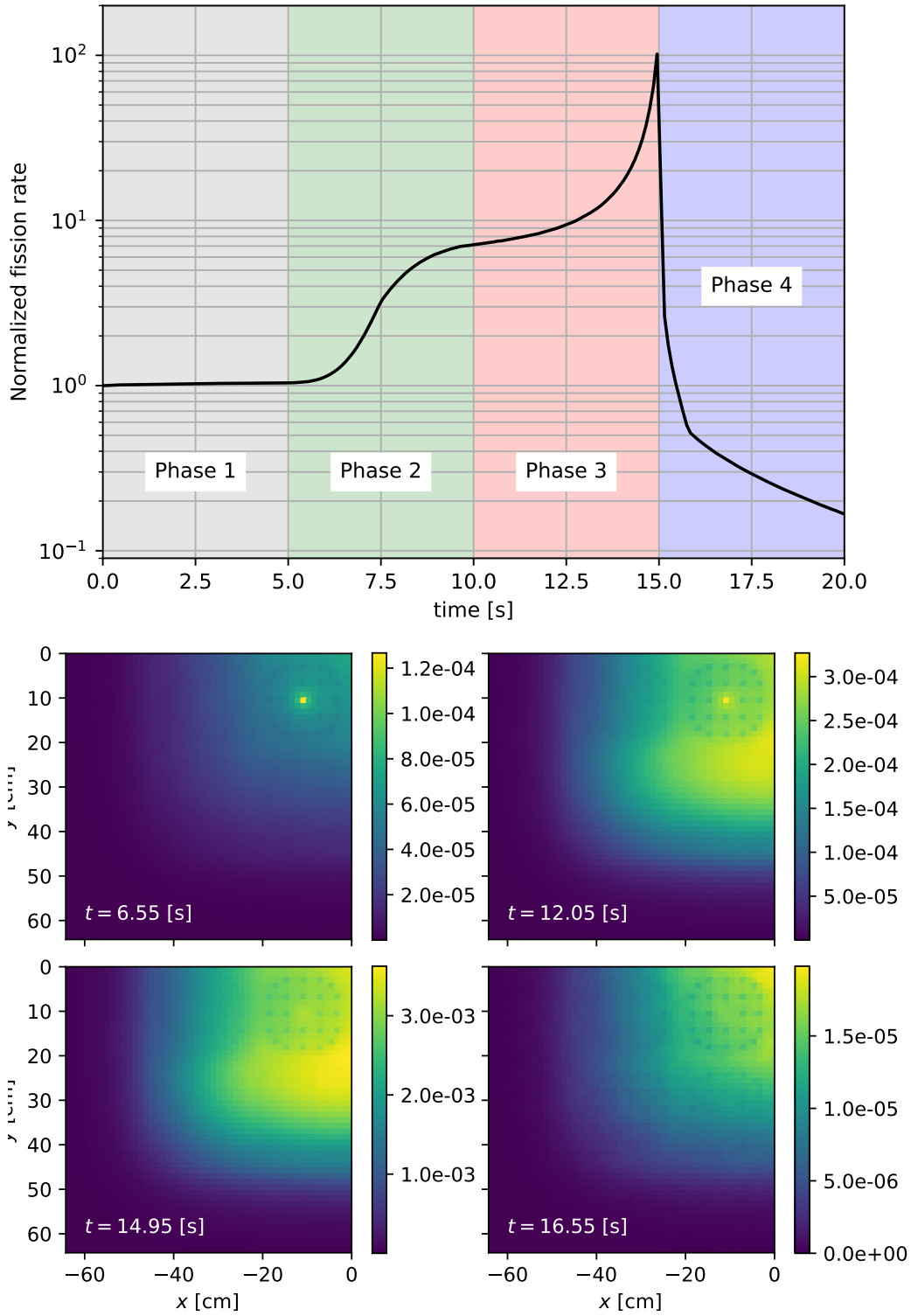


Figure 10: C5G7 stuck rod accident simulation: (above) flux densities through time showing the four phases shaded as gray, green, red, and blue respectively; (below) scalar flux on  $x$ - $y$  plane (top view) at points in time.

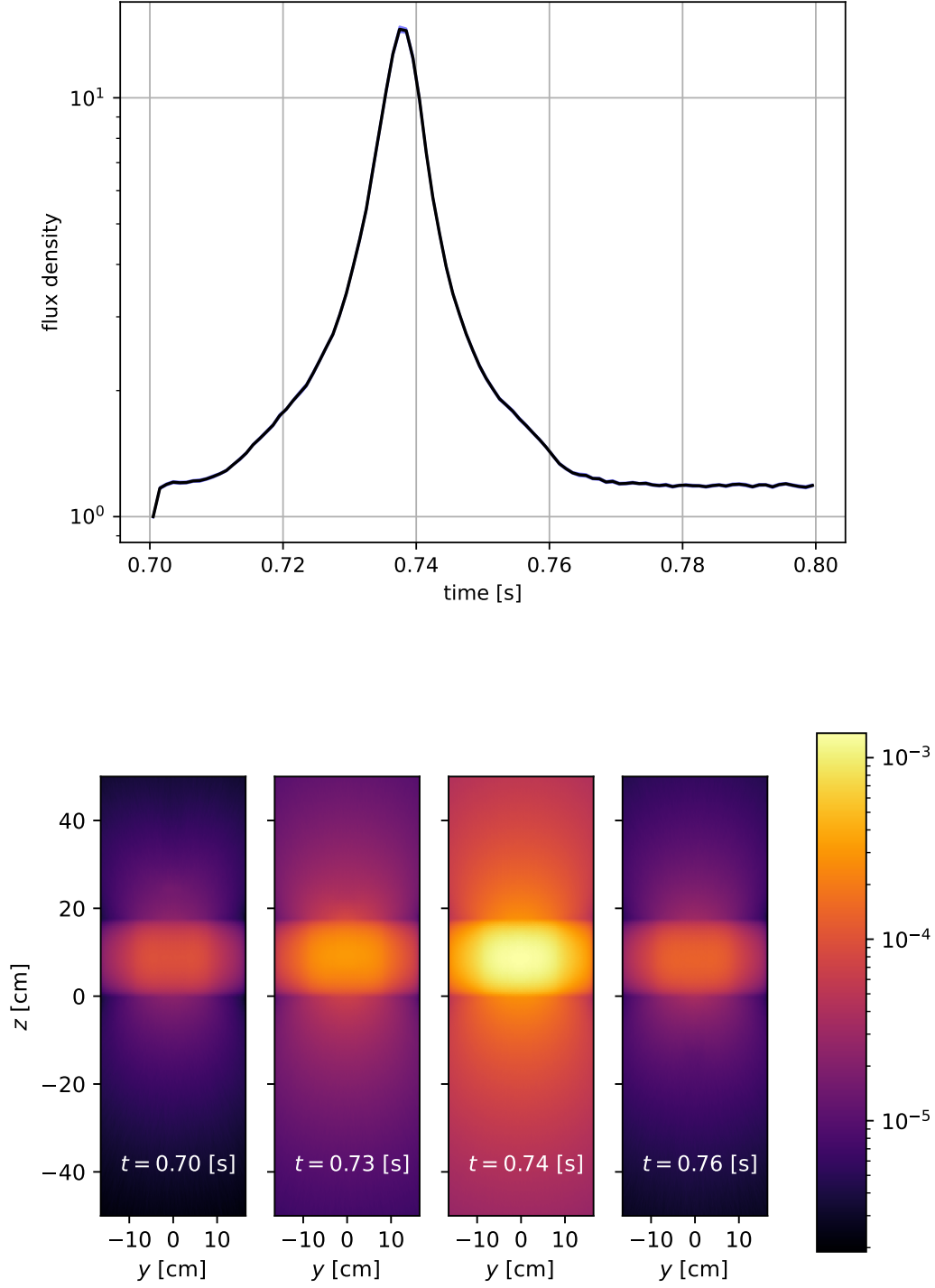


Figure 11: Dragon burst simulation: (above) flux density as a function of time, (below) scalar flux on  $y$ - $z$  plane (side view) at points in time.

| Problem  | Tracking Alg.      | Estimator | Runtime [s] | $\ \hat{\sigma}^2\ _1$ | Figure of Merit |
|----------|--------------------|-----------|-------------|------------------------|-----------------|
| Kobyashi | surface            | TLE       | 1574        | $4.514 \times 10^{-3}$ | 0.1407          |
|          | surface            | CE        | 1014        | $9.552 \times 10^{-2}$ | 0.0103          |
|          | delta              | TLE       | 1298        | $4.539 \times 10^{-3}$ | 0.1697          |
|          | delta              | CE        | 817.2       | $2.062 \times 10^{-1}$ | 0.0059          |
| C5G7     | surface            | TLE       | 7926        | $1.295 \times 10^{-4}$ | 0.9744          |
|          | surface            | CE        | 3173        | $1.295 \times 10^{-4}$ | 2.4336          |
|          | delta              | TLE       | 2870        | $1.400 \times 10^{-4}$ | 2.4889          |
|          | delta              | CE        | 1820        | $2.152 \times 10^{-4}$ | 2.5515          |
| C5CE     | surface            | TLE       | 734.6       | $1.812 \times 10^{-3}$ | 0.7484          |
|          | surface            | CE        | 587.8       | $1.812 \times 10^{-3}$ | 0.9391          |
|          | delta              | TLE       | 496.8       | $4.906 \times 10^{-3}$ | 0.4103          |
|          | delta              | CE        | 555.0       | $1.173 \times 10^{-2}$ | 0.1536          |
|          | hybrid-energy      | TLE       | 226.25      | $1.164 \times 10^{-3}$ | 3.798           |
|          | hybrid-energy      | CE        | 220.5       | $1.144 \times 10^{-3}$ | 3.965           |
| Dragon   | surface            | TLE       | 3816        | $1.163 \times 10^{-6}$ | 221.4           |
|          | delta              | CE        | DNF*        | -                      | -               |
|          | delta              | TLE       | DNF*        | -                      | -               |
|          | hybrid-in-material | TLE       | 15 493      | $1.106 \times 10^{-6}$ | 58.40           |

Table 2: Results for benchmark problems on Dane (112× Intel Sapphire Rapids CPU cores). \*Did not finish in eight-hour time limit.

surface tracking is most pronounced in problems with many surface crossings [2]. Our objectives of comparing delta tracking methods for this specific problem are to confirm that delta tracking works with such a dynamic problem with continuously moving materials and to assess whether the hybrid-in-material method outperforms standard delta tracking.

## 6 Results

In this section, we discuss the performance results of the benchmarks modeled with surface, delta, and voxelized delta tracking, as well as the hybrid-in-energy and hybrid-in-material tracking algorithms. We also verify that the various delta tracking methods converge to the same solution as surface tracking when transporting on a geometry with continuously moving surfaces.

### 6.1 Performance results

All results presented below are executed on the Dane and Lassen high-performance computing systems at Lawrence Livermore National Laboratory (LLNL). Dane is a CPU-only system with dual-socket Intel Xeon Sapphire Rapids CPUs, each with 56 cores for a total of 112 CPU cores per node. Lassen is the open collaboration sibling to the Sierra machine with four Nvidia Tesla V100 GPUs and two IBM Power 9 CPUs per node. We make all performance statements with respect to a whole node of Dane (112 MPI threads, CPU) and a whole node of Lassen (4 MPI threads, GPU). We compile to CPUs with Numba v0.60.0, and compile to Nvidia GPUs with CUDA v11.8 and Nvidia-PTX with Numba v0.59.0<sup>1</sup>. The delta tracking methods are built using MC/DC v0.12.0 [25], compiling on GPUs with Harmonize v0.0.2 [39]. All floating-point operations use double precision.

Tables 2 and 3 show the wall clock runtimes,  $L_1$  norm of the Monte Carlo variance ( $\|\hat{\sigma}^2\|_1$ ), and figures of merit (FoM) for benchmark problems using various transport algorithms and flux estimators on the Dane and Lassen machines, respectively.

<sup>1</sup>Numba v0.59.1 is the most recent version to support Power9 CPUs.

| Problem   | Tracking Alg.   | Estimator | Runtime [s] | $\ \hat{\sigma}^2\ _1$ | Figure of Merit |
|-----------|-----------------|-----------|-------------|------------------------|-----------------|
| Kobayashi | surface         | TLE       | 973.9       | $4.514 \times 10^{-3}$ | 0.2275          |
|           | surface         | CE        | 840.6       | $9.952 \times 10^{-2}$ | 0.0125          |
|           | delta           | TLE       | 831.8       | $4.539 \times 10^{-3}$ | 0.2649          |
|           | delta           | CE        | 620.7       | $2.062 \times 10^{-1}$ | 0.0078          |
| C5G7      | surface         | TLE       | 4598        | $1.305 \times 10^{-4}$ | 1.666           |
|           | surface         | CE        | 2403        | $1.305 \times 10^{-4}$ | 3.1878          |
|           | delta           | TLE       | 1615        | $1.400 \times 10^{-4}$ | 4.4205          |
|           | delta           | CE        | 789.3       | $2.152 \times 10^{-4}$ | 5.8860          |
| C5CE      | surface         | TLE       | 550.9       | $2.452 \times 10^{-3}$ | 0.7402          |
|           | surface         | CE        | 465.9       | $2.452 \times 10^{-3}$ | 0.8753          |
|           | delta           | TLE       | 500.7       | $1.690 \times 10^{-2}$ | 0.1182          |
|           | delta           | CE        | 421.6       | $1.793 \times 10^{-2}$ | 0.1323          |
|           | hybrid-energy   | TLE       | 291.7       | $1.557 \times 10^{-3}$ | 2.2023          |
|           | hybrid-energy   | CE        | 275.6       | $1.839 \times 10^{-3}$ | 1.9731          |
| Dragon    | surface         | TLE       | 3993        | $1.163 \times 10^{-6}$ | 2153            |
|           | delta           | CE        | DNF*        | -                      | -               |
|           | delta           | TLE       | DNF*        | -                      | -               |
|           | hybrid-material | TLE       | DNF*        | -                      | -               |

Table 3: Results for benchmark problems on Lassen (4× Nvidia Tesla V100). \*Did not finish in eight-hour time limit.

On Dane, delta tracking and a collision estimator dramatically improve runtime for the Kobayashi problem compared with surface tracking, with a collision or track length estimator. However, this speedup does not compensate for the two orders of magnitude additional variance on the tallies of interest incurred by the collision estimator. This leads to a significantly smaller figure of merit for standard delta tracking and surface tracking (using a collision estimator) compared with results from the track length estimator. Figure 12 shows the simulated flux at various points in time for the Kobayashi problem computed using standard delta tracking with a collision estimator (bottom) and voxelized delta tracking (top). The collision estimator yields a solution with a higher variance (appearing as static) result compared to that of the track length estimator. The voxelized tally method achieves a 21% decrease in wall clock time for the same amount of normed variance, leading to a moderately improved figure of merit (0.1697 and 0.1407 for the voxelized method and surface tracking, respectively). On GPUs, the pattern is the same, with the voxelized method performing slightly better than surface tracking with a track length estimator. All algorithms run between 1.2× and 1.7× faster on Lassen than Dane.

For C5G7 on Dane, standard delta tracking performs the best with similar L1 norm of variance (1820s and  $2.152 \times 10^{-4}$ , respectively). Surface tracking sees the longest runtime and voxelized delta tracking sits between the two (7926s and 2870s, respectively) with roughly the same error ( $1.3 \times 10^{-4}$ ). For C5G7, there does not appear to be a benefit in using the track length estimator. This pattern is also observed in the Lassen results, with between 1.7× and 2× wall clock runtime speedup for all tracking methods when moving from Dane to Lassen, while the variance remains about the same. Voxelized delta tracking shows a 2.6× and 2.7× higher figure of merit over surface tracking on Dane and Lassen, respectively, and standard delta tracking performs slightly better than the voxelized tally method.

In solving the C5CE problem, surface tracking methods yielded the highest figures of merit, with the collision and track length estimator. The speedup of Lassen over Dane is now lower (between 0.9× and 1.3×), indicating improvements are needed for our continuous energy physics when implemented on GPUs. The hybrid-in-energy method provides significant improvement in FoM with an order of magnitude increase: 11× on Dane, 7× on Lassen. The use of the collision estimator in the hybrid

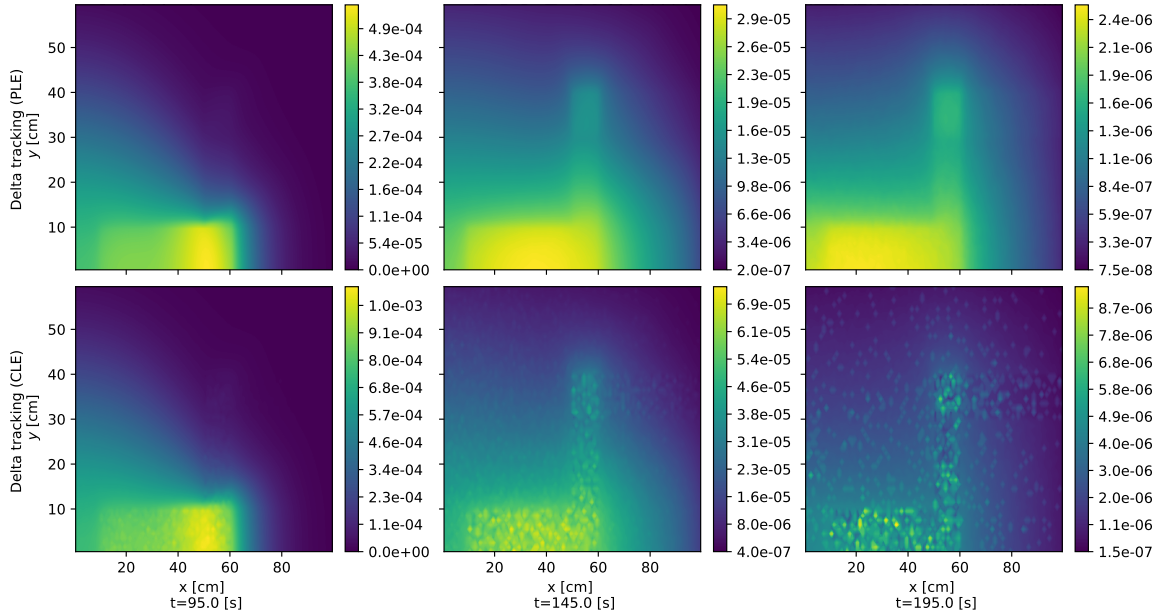


Figure 12: Comparison of delta tracking using the track length estimator (top row) and collision estimator (bottom row) at three points in time. The solution produced with the collision estimator has much higher variance.

method slightly outperforms the use of the track length estimator.

The performance of the methods on the Dragon problem is at odds with observations of the algorithms on the other problems. Delta tracking simulations (both standard and voxelized) do not reach the end of the specified end time on Dane or Lassen in the eight hours allocated, on either machine. On Dane, as predicted, the hybrid-in-material method improves performance over the other two methods, as it completes the simulation in about four hours. However, standard surface tracking requires only one hour for this simulation. The hybrid-in-material method did not finish on Lassen. These observations are consistent with the understanding that delta tracking is typically less effective for problems with fewer surfaces and significant material heterogeneities.

## 7 Discussion, Conclusions, and Future Work

We have implemented delta tracking in MC/DC on CPUs and GPUs, including using a voxelized track length tally to efficiently score scalar flux. We verify the solution produced by this method against various steady-state and time-dependent analytic benchmark problems available in the MC/DC verification suite. We also verify that delta tracking functions properly with continuously moving surfaces in MC/DC using the fuel pellet problem. Figures of merit improve modestly in large-scale multi-group and continuous energy time-dependent benchmark problems when using this tracking and tallying technique on CPUs and GPUs.

We have also demonstrated a novel hybrid-in-energy surface-delta tracking scheme, where surface and delta tracking are used at low and high energies, respectively. On the continuous energy version of the C5G7 benchmark geometry undergoing a four-phase transient, we observe an order of magnitude increase in FOM with the hybrid-in-energy scheme, on both CPU and GPU nodes. We have also confirmed that hybrid surface-delta tracking methods can yield improved results in problems with significant void regions [9].

An efficient Monte Carlo algorithm is a combination of a numerical method that obtains a lower variance with fewer particles and an efficient implementation of that numerical method. What makes a given delta or surface tracking algorithm more or less “efficient” can vary code-to-code depending on the optimizations software developers have chosen. Not every code implements tallying the same



way as MC/DC, meaning the added efficiency of using the voxelized tally may not be a viable option in other Monte Carlo neutron transport codes.

The main takeaway of this work is that delta and surface tracking do not have to be treated as discrete choices in the numerical method, as corroborated by papers from the developers of Serpent2 and MONK/MCBEND [4, 10]. Greater performance can potentially be achieved by mixing and matching the underlying transport methods, given the physical parameters of a simulation and the relative strengths and weaknesses of a given transport application. As discussed in Section 3.4, implementing delta tracking in a surface tracking code is relatively simple, given a method to calculate a macroscopic majorant cross section.

The use of the voxelized tally method in void regions is promising, but the lack of reaction rate tallies limits its applicability. Work is ongoing to produce efficient methods of computing relevant macroscopic cross sections defined on a structured mesh while a particle is undergoing transport. This process is straightforward for multi-group cross sections where reaction rates can be determined entirely via post-processing, but we are working to identify the most efficient method for continuous energy transport.

Methods for reducing the dimensionality of the majorant are also being explored to achieve a more-efficient majorant cross section lookup in distance to collision operations. Experiments with the collision estimator for scalar flux and methods of tallying into vacuum and low interaction rate regions are being considered, including implementing a cutoff method [9] or weighted delta tracking [3].

## Acknowledgments

We thank Patrick Shriwise and Paul Romano of Argonne National Laboratory, Mike Rising of Los Alamos National Laboratory, Jaakko Leppänen of VTT Technical Research Center of Finland, and Simon Richards of ANSWERS software for productive conversations. We also thank the high performance computing staff at Lawrence Livermore National Laboratory for continued support using the Dane machine.

This work was supported by the Center for Exascale Monte-Carlo Neutron Transport (CEMeNT) a PSAAP-III project funded by the Department of Energy, grant number: DE-NA003967.

## References

- [1] E. E. Lewis and W. F. Miller, *Computational Methods of Neutron Transport*. New York, NY: Wiley, 1984.
- [2] E. R. Woodcock, T. Murphy, P. Hemmings, and T. C. Longworth, “Techniques used in the GEM code for Monte Carlo neutronics calculations in reactors and other systems of complex geometry,” United Kingdom Atomic Energy Authority, Risley, Warrington, Lancs., England, Tech. Rep., 1965.
- [3] L. Morgan and D. Kotlyar, “Weighted-delta-tracking for Monte Carlo particle transport,” *Annals of Nuclear Energy*, vol. 85, pp. 1184–1188, nov 2015. DOI:10.1016/j.anucene.2015.07.038
- [4] J. Leppänen, “On the use of delta-tracking and the collision flux estimator in the Serpent 2 Monte Carlo particle transport code,” *Annals of Nuclear Energy*, vol. 105, pp. 161–167, Jul. 2017. DOI:10.1016/j.anucene.2017.03.006
- [5] R. G. McClarren, *Computational Nuclear Engineering and Radiological Science Using Python*. Cambridge, USA: Elsevier, 2018.
- [6] B. Molnar, G. Tolnai, and D. Legrady, “Variance Reduction and Optimization Strategies in a Biased Woodcock Particle Tracking Framework,” *Nuclear Science and Engineering*, vol. 190, no. 1, pp. 56–72, Apr. 2018. DOI:10.1080/00295639.2017.1413876

- [7] J. P. Morgan, T. J. Trahan, T. P. Burke, C. J. Josey, and K. E. Niemeyer, “Hybrid-Delta Tracking on a Structured Mesh in MCATK,” in *Proceedings of the International Conference on Mathematics and Computational Methods Applied to Nuclear Science and Engineering (M&C 2023)*. CNS, 2023. DOI:10.48550/arXiv.2306.07847
- [8] J. Leppänen, “Development of a dynamic simulation mode in Serpent 2 Monte Carlo code,” in *Proceedings of the International Conference on Mathematics and Computational Methods Applied to Nuclear Science and Engineering (M&C 2013)*, 2013.
- [9] J. Leppänen, “Performance of Woodcock delta-tracking in lattice physics applications using the Serpent Monte Carlo reactor physics burnup calculation code,” *Annals of Nuclear Energy*, vol. 37, no. 5, pp. 715–722, May 2010. DOI:10.1016/j.anucene.2010.01.011
- [10] S. D. Richards *et al.*, “MONK and MCBEND: Current status and recent developments,” *Annals of Nuclear Energy*, vol. 82, pp. 63–73, Aug. 2015. DOI:10.1016/j.anucene.2014.07.054
- [11] J. P. Morgan *et al.*, “Monte Carlo / Dynamic Code (MC/DC): An accelerated Python package for fully transient neutron transport and rapid methods development,” *Journal of Open Source Software*, vol. 9, no. 96, p. 6415, Apr. 2024. DOI:10.21105/joss.06415
- [12] S. Pasmann, I. Variansyah, C. T. Kelley, and R. McClarren, “A Quasi-Monte Carlo Method With Krylov Linear Solvers for Multigroup Neutron Transport Simulations,” *Nuclear Science and Engineering*, vol. 197, no. 6, pp. 1159–1173, 2023. DOI:10.1080/00295639.2022.2143704
- [13] S. Pasmann, I. Variansyah, C. T. Kelley, and R. G. McClarren, “Mitigating Spatial Error in the Iterative Quasi-Monte Carlo (iQMC) Method for Neutron Transport Simulations with Linear Discontinuous Source Tilting and Effective Scattering and Fission Rate Tallies,” *Nuclear Science and Engineering*, vol. 199, no. sup1, pp. S381–S396, 2025. DOI:10.1080/00295639.2024.2332007
- [14] I. Lux, *Monte Carlo Particle Transport Methods*. CRC Press, 1991.
- [15] M. Rising *et al.*, “MCNP<sup>®</sup> Code Version 6.3.0 Release Notes,” Los Alamos National Laboratory, Los Alamos, NM, USA, Tech. Rep. LA-UR-22-33103, Rev. 1, January 2023.
- [16] S. P. Hamilton and T. M. Evans, “Continuous-energy Monte Carlo neutron transport on GPUs in the Shift code,” *Annals of Nuclear Energy*, vol. 128, pp. 236–247, Jun. 2019. DOI:10.1016/j.anucene.2019.01.012
- [17] T. M. Pandya, S. R. Johnson, T. M. Evans, G. G. Davidson, S. P. Hamilton, and A. T. Godfrey, “Implementation, capabilities, and benchmarking of Shift, a massively parallel Monte Carlo radiation transport code,” *Journal of Computational Physics*, vol. 308, pp. 239–272, 2016. DOI:10.1016/j.jcp.2015.12.037
- [18] Heinrichs, David, Lent, Edward, and Lee, Chuck, “COG 11.3 New Features,” *EPJ Nuclear Sci. Technol.*, vol. 11, p. 2, 2025. Available: <https://doi.org/10.1051/epjn/2024017>. DOI:10.1051/epjn/2024017
- [19] Hugot, François-Xavier *et al.*, “Overview of the TRIPOLI-4 Monte Carlo code, version 12,” *EPJ Nuclear Sci. Technol.*, vol. 10, p. 17, 2024. DOI:10.1051/epjn/2024018
- [20] P. K. Romano, N. E. Horelik, B. R. Herman, A. G. Nelson, B. Forget, and K. Smith, “OpenMC: A state-of-the-art Monte Carlo code for research and development,” *Annals of Nuclear Energy*, vol. 82, pp. 90–97, Aug. 2015. DOI:10.1016/j.anucene.2014.07.048
- [21] J. Leppänen, M. Pusa, T. Viitanen, V. Valtavirta, and T. Kaltiaisenaho, “The Serpent Monte Carlo code: Status, development and applications in 2013,” *Annals of Nuclear Energy*, vol. 82, pp. 142–150, 2015. DOI:10.1016/j.anucene.2014.08.024

- [22] P. Fang *et al.*, “Development and preliminary verification of a Monte Carlo neutron transport code IMPC-Neutron,” *Annals of Nuclear Energy*, vol. 175, pp. 109–221, 2022. DOI:10.1016/j.anucene.2022.109221
- [23] B. Molnar, G. Tolnai, and D. Legrady, “A GPU-based direct Monte Carlo simulation of time dependence in nuclear reactors,” *Annals of Nuclear Energy*, vol. 132, pp. 46–63, Oct. 2019. DOI:10.1016/j.anucene.2019.03.024
- [24] S. D. Richards, J. A. Fildes, R. P. Hiles, B. J. Jones, and P. N. Smith, “Advances in Stochastic Geometry Modelling in MONK and MCBEND, the Importance of Stochastic Models, and an Approach to Validation,” in *Proceedings of the International Conference on Mathematics and Computational Methods Applied to Nuclear Science and Engineering (M&C 2025)*. ANS, 2023. DOI:10.48550/arXiv.2306.07847
- [25] I. Variansyah *et al.*, “MC/DC: Monte Carlo Dynamic Code version 0.11.1,” Oct. 2024. Available: <https://doi.org/10.5281/zenodo.14010170>
- [26] B. Ganapol, R. Baker, J. Dahl, and R. E. Alcouffe, “Homogeneous Infinite Media Time-Dependent Analytical Benchmarks,” in *International Meeting on Mathematical Methods for Nuclear Applications*, vol. 41(25), Salt Lake City, UT, 9 2001.
- [27] N. Hfaiedh and A. Santamarina, “Determination of the optimized SHEM mesh for neutron transport calculations,” in *Proceedings of the International topical meeting on mathematics and computation, supercomputing, reactor physics and nuclear and biological applications*, Jul 2005.
- [28] W. H. R. and, “New Difference Schemes for the Neutron Transport Equation,” *Nuclear Science and Engineering*, vol. 46, no. 2, pp. 309–314, 1971. DOI:10.13182/NSE46-309
- [29] J. Duderstadt and L. Hamilton, *Nuclear Reactor Analysis*. New York, NY, USA: John Wiley and Sons, Inc., 1974.
- [30] J. J. Hou, K. N. Ivanov, V. F. Boyarinov, and P. A. Fomichenko, “OECD/NEA benchmark for time-dependent neutron transport calculations without spatial homogenization,” *Nuclear Engineering and Design*, vol. 317, pp. 177–189, 2017. DOI:10.1016/j.nucengdes.2017.02.008
- [31] I. Variansyah, J. P. Morgan, J. Northrop, K. E. Niemeyer, and R. G. McClarren, “Development of MC/DC: a performant, scalable, and portable Python-based Monte Carlo neutron transport code,” in *International Conference on Mathematics and Computational Methods Applied to Nuclear Science and Engineering*, Niagara Falls, Ontario, Canada, 2023. DOI:10.48550/arXiv.2305.07636
- [32] B. Cuneo and M. Bailey, “Divergence Reduction in Monte Carlo Neutron Transport with On-GPU Asynchronous Scheduling,” *ACM Trans. Model. Comput. Simul.*, 10 2023, just Accepted. DOI:10.1145/3626957
- [33] J. P. Morgan, I. Variansyah, B. Cuneo, T. S. Palmer, and K. E. Niemeyer, “Performant and Portable Monte Carlo Neutron Transport via Numba,” *Computing in Science & Engineering*, pp. 1–10, 2025. DOI:10.1109/MCSE.2025.3550863
- [34] B. Cuneo, J. P. Morgan, I. Variansyah, and K. E. Niemeyer, “Comparing the Performance of MC/DC’s on-GPU Event-based Processing Methods in Multigroup and Continuous-energy Problems,” in *Proceedings of the International Conference on Mathematics and Computational Methods Applied to Nuclear Science and Engineering (M&C 2025)*, 2025. DOI:10.13182/MC25-47174
- [35] K. Kobayashi, N. Sugimura, and Y. Nagaya, “3D radiation transport benchmark problems and results for simple geometries with void region,” *Progress in Nuclear Energy*, vol. 39, pp. 119–144, 2001. DOI:10.1016/S0149-1970(01)00007-5

- [36] I. Variansyah, “Time-Dependent Kobayashi Dog-Leg Benchmark for Neutron Transport,” <https://doi.org/10.5281/zenodo.15069882>, Mar. 2025.
- [37] R. Kimpland, T. Grove, P. Jaegers, R. Malenfant, and W. M. and, “Critical Assemblies: Dragon Burst Assembly and Solution Assemblies,” *Nuclear Technology*, vol. 207, no. sup1, pp. S81–S99, 2021. DOI:10.1080/00295450.2021.1927626
- [38] I. Variansyah and R. G. McClarren, “High-fidelity treatment for object movement in time-dependent Monte Carlo transport simulations,” in *Proceedings of the International Conference on Mathematics and Computational Methods Applied to Nuclear Science and Engineering (M&C 2023)*. CNS, 2023. Available: <https://arxiv.org/abs/2305.07641>
- [39] Center for Exascale Monte Carlo Neutron Transport (CEMeNT), B. Cuneo, and J. P. Morgan, “Harmonize version 0.0.2,” Apr. 2024. Available: <https://doi.org/10.5281/zenodo.14019208>
- [40] S. Van Der Walt, S. C. Colbert, and G. Varoquaux, “The NumPy Array: A Structure for Efficient Numerical Computation,” *Computing in Science & Engineering*, vol. 13, no. 2, pp. 22–30, Mar. 2011. DOI:10.1109/MCSE.2011.37
- [41] P. Virtanen *et al.*, “SciPy 1.0: Fundamental Algorithms for Scientific Computing in Python,” *Nature Methods*, vol. 17, pp. 261–272, 2020. DOI:10.1038/s41592-019-0686-2

## A Continuous Energy Macroscopic Majorant

To compute a unified energy grid per material, we combine the energy grids from all nuclides in a given material. Then we call `numpy.unique()`, which returns a sorted array (from smallest to largest) with no repeating elements [40]. To compute a unified energy grid for the whole problem, we do the same but with all the nuclides in the entire problem.

Computing a macroscopic majorant for nuclides that are not on a unified energy grid requires two levels of interpolation to put a given macroscopic total cross section on a unified energy grid. First, interpolate from each nuclide's microscopic cross section onto a material's unified energy grid to compute a macroscopic total cross section. Then, perform a second interpolation from the material to the majorant's unified energy grid. We use `scipy.interpolate.interp1d()` to interpolate from one energy grid to the next [41].

The following code shows how this is done in MC/DC:

```
1 import scipy
2 import numpy
3
4 # unify the energy grids from all nuclides
5 majorant_energy_grid = np.array([])
6 for n in range(N_nuclide):
7     nuclide = mcdc["nuclides"][n]
8     majorant_energy_grid = np.append(majorant_energy_grid, nuclide["E_xs"])
9
10 # sort energy grid and eliminate duplicate points
11 majorant_energy_grid = np.unique(majorant_energy_grid)
12 majorant_xsec = np.zeros_like(majorant_energy_grid)
13
14 for m in range(N_material):
15
16     material = mcdc["materials"][m]
17
18     material_energy_grid = np.array([])
19
20     # compute a unified energy grid across all nuclides of a given material
21     for n in range(material["N_nuclide"]):
22         nuclide = mcdc["nuclides"][n]
23         material_energy_grid = np.append(
24             material_energy_grid, nuclide["E_xs"]
25         )
26     material_energy_grid = np.unique(material_energy_grid)
27     MacroXS = np.zeros_like(material_energy_grid)
28
29     # compute the macroscopic total cross section of a material on its unified
30     # energy grid
31     for n in range(material["N_nuclide"]):
32         ID_nuclide = material["nuclide_IDs"][n]
33         nuclide = mcdc["nuclides"][ID_nuclide]
34
35         # Get nuclide density
36         N = material["nuclide_densities"][n]
37
38         # putting the microscopic cross-sections on the unified
39         # material energy grid
40         total_micro_xsec_unified = scipy.interpolate.interp1d(
41             nuclide["E_xs"], nuclide["ce_total"], bounds_error=False
```

```

42     )
43     total_micro_xsec_unified = total_micro_xsec_unified(
44         material_energy_grid
45     )
46
47     # Accumulate
48     MacroXS += N * total_micro_xsec_unified
49
50     # putting the total macroscopic cross sections on on the majorant energy grid
51     total_xsec_unified = scipy.interpolate.interp1d(
52         material_energy_grid, MacroXS, bounds_error=False
53     )
54     total_xsec_unified = total_xsec_unified(majorant_energy_grid)
55
56     # compares old majorant xsec and the currently evaluated unified xsec
57     # and picks the larger xsecs
58     majorant_xsec = np.max((majorant_xsec, total_xsec_unified), axis=0)
59

```

This process results in a large majorant cross-section that is very large. Other, more efficient algorithms exist to produce a similarly accurate majorant with fewer points. Delta tracking codes like Serpent2, GUARDYAN, and IMPC avoid the need for energy grid unification by having all nuclides on a unified energy grid in their data library [21, 23, 22].

## B C5CE Material Definition

| Material             | Nuclide                      | Atom fraction                              |
|----------------------|------------------------------|--|
| UO <sub>2</sub> Fuel | O-16                         | 0.045 852 653 893 777 34                   |
|                      | O-17                         | 1.741 960 403 157 433 8 × 10 <sup>-5</sup> |
|                      | O-18                         | 9.194 241 663 525 41 × 10 <sup>-5</sup>    |
|                      | U-235                        | 0.000 721 748 604 118 994 7                |
|                      | U-238                        | 0.022 249 502 307 202 95                   |
| MOX-43 Fuel          | O-17                         | 1.743 649 552 488 715 × 10 <sup>-5</sup>   |
|                      | O-16                         | 0.045 897 116 431 227 53                   |
|                      | O-17                         | 1.743 649 552 488 715 × 10 <sup>-5</sup>   |
|                      | O-18                         | 9.203 157 163 056 531 × 10 <sup>-5</sup>   |
|                      | U-235                        | 0.000 375 026 416 877 241 4                |
|                      | U-238                        | 0.022 623 195 992 286 36                   |
| MOX-7 Fuel           | O-16                         | 0.045 830 366 141 582 77                   |
|                      | O-17                         | 1.741 113 682 662 514 × 10 <sup>-5</sup>   |
|                      | O-18                         | 9.189 772 587 857 765 × 10 <sup>-5</sup>   |
|                      | U-235                        | 0.000 558 138 230 289 339 6                |
|                      | U-238                        | 0.022 404 154 012 604 437                  |
| MOX-87 Fuel          | O-16                         | 0.045 852 653 893 777 34                   |
|                      | O-17                         | 1.741 960 403 157 433 8 × 10 <sup>-5</sup> |
|                      | O-18                         | 9.194 241 663 525 41 × 10 <sup>-5</sup>    |
|                      | U-235                        | 0.000 721 748 604 118 994 7                |
|                      | U-238                        | 0.022 249 502 307 202 95                   |
| Guide Tube           | H-1                          | 0.050 347 844 752 850 625                  |
|                      | H-2                          | 7.842 394 716 362 082 × 10 <sup>-6</sup>   |
|                      | O-16                         | 0.025 117 935 412 784 034                  |
|                      | O-17                         | 9.542 402 714 463 945 × 10 <sup>-6</sup>   |
|                      | O-18                         | 5.036 575 828 499 65 × 10 <sup>-5</sup>    |
| Fission Chamber      | H-1                          | 0.050 347 844 752 850 625                  |
|                      | H-2                          | 7.842 394 716 362 082 × 10 <sup>-6</sup>   |
|                      | O-16                         | 0.025 117 935 412 784 034                  |
|                      | O-17                         | 9.542 402 714 463 945 × 10 <sup>-6</sup>   |
|                      | O-18                         | 5.036 575 828 499 65 × 10 <sup>-5</sup>    |
| Control Rod          | Ag-107                       | 0.023 523 285 675 833 942                  |
|                      | Ag-109                       | 0.021 854 298 142 978 04                   |
|                      | In-113                       | 0.000 342 192 204 265 564 4                |
|                      | In-115                       | 0.007 651 085 167 039 375                  |
|                      | Cd-106                       | 3.388 162 764 513 86 × 10 <sup>-5</sup>    |
|                      | Cd-108                       | 2.416 617 297 099 042 5 × 10 <sup>-5</sup> |
|                      | Cd-110                       | 0.000 339 360 559 626 408 3                |
|                      | Cd-111                       | 0.000 348 205 161 220 520 8                |
|                      | Cd-112                       | 0.000 656 106 153 330 639 8                |
|                      | Cd-113                       | 0.000 332 747 519 049 887 26               |
|                      | Cd-114                       | 0.000 782 515 920 729 570 5                |
| Cd-116               | 0.000 204 432 760 538 378 45 |  |
| Moderator            | H-1                          | 0.050 347 844 752 850 625                  |
|                      | H-2                          | 7.842 394 716 362 082 × 10 <sup>-6</sup>   |
|                      | O-16                         | 0.025 117 935 412 784 034                  |
|                      | O-17                         | 9.542 402 714 463 945 × 10 <sup>-6</sup>   |

O-18  $5.036\,575\,828\,499\,65 \times 10^{-5}$

---

Table 4: Materials used in C5CE problem